



A STRAIN-GRADIENT MODEL OF CLEAVAGE FRACTURE IN PLASTICALLY DEFORMING MATERIALS

D. M. LIPKIN¹, D. R. CLARKE¹ and G. E. BELTZ²

¹Materials Department and ²Department of Mechanical & Environmental Engineering, University of California, Santa Barbara, CA 93106, U.S.A.

(Received 16 October 1995; in revised form 12 January 1996)

Abstract—The current analysis presents a model for cleavage fracture in the presence of dislocation plasticity. We build on a framework developed in an earlier paper [Lipkin *et al.*, *Acta mater.* **44**, 1287 (1996)], wherein an elastic core is embedded about the crack tip in a plastically deforming medium. This model provides a mechanism by which cleavage-type crack growth could proceed concomitantly with significant plastic dissipation. The present model is amended to account for the large strain gradients in the immediate vicinity of the crack tip. Such gradients are thought to lead to extensive local hardening. A simple, continuum-based model is used to identify a characteristic length scale ahead of the crack tip, within which the material cannot plastically deform subject to the crack-tip stress field. An expression is derived for the crack-tip shielding afforded by the plasticity prior to initiation of fracture. The strong dependence of toughness on the ideal work of fracture indicates a possible mechanism for such varied phenomena as segregation-induced embrittlement, ductile-to-brittle transition, stress corrosion cracking and constrained fracture in metal-ceramic composites. Copyright © 1996 Acta Metallurgica Inc.

1. INTRODUCTION

Early fracture models drew a sharp distinction between "brittle" and "ductile" fracture. Ideally brittle (or Griffith) fracture is based on the balance between the elastic energy stored in a cracked body (with its surrounding loading system) and the energy associated with the newly created fracture surfaces [1]. By contrast, fully plastic fracture is typically characterized by crack-tip blunting and hole growth [2, 3]. In practice, however, fracture processes can generally exhibit characteristics attributable to both types of behavior. Orowan's assertion that the Griffith criterion for brittle fracture be modified to include the plastic work dissipated in the crack-tip process zone [4] was the first attempt to bridge the gap between ductile and brittle fracture models. Rice's recognition that the amount of plastic work dissipated during the fracture process has a strong functional dependence on the surface (or Griffith) energy itself (the "valve" effect) [5] further emphasized the importance of plasticity in nominally brittle fracture processes. Quantification of this valve effect, culminating in a relation between atomic-scale decohesion and large-scale plastic dissipation, is the motivation for our present work.

Segregation-induced interfacial embrittlement in metals and metal-ceramic couples [6, 7] is a prime example of the strong role played by plastic dissipation in an otherwise cleavage-type fracture. Previous attempts at quantifying the valve effect, notably those by Thomson [8], Suo *et al.* [9] and Jokl *et al.* [10], have identified the existence of the

inherently nonlinear coupling between the crack-tip decohesion and the surrounding plastic deformation. However, these models fall short of a self-consistent description of the fracture process in terms of measurable material parameters. In an earlier paper [11], we presented a simple model that quantified the coupling between the Griffith energy and the plastic work in terms of the interfacial work of adhesion, yield strength and work-hardening exponent. Although this approach provides valuable insight into the interaction between two processes occurring on drastically different length scales, there is an underlying—and somewhat tenuous—assumption that a relatively large ($\sim 1 \mu\text{m}$) dislocation-free core exists at the crack tip. Presently, we reformulate our model in the context of strain-gradient plasticity theory, lifting the requirement of a dislocation-free core. In so doing, we arrive at an inherent material length scale within which dislocation plasticity is inhibited and at the shielding ratio of the macroscopically measured toughness to the work of adhesion.

2. THE MODEL

2.1. The plastic zone

Figure 1 illustrates the physical basis for the following discussion. A plastically deforming body containing a pre-existing, sharp crack is loaded in opening mode by remote tractions, allowing for a plastic zone to develop about the crack tip. The material surrounding the crack tip is allowed to plastically deform and strain harden, following the

large-strain limit of the generalized Ramberg-Osgood constitutive law

$$\bar{\sigma}_{\text{flow}} = \sigma_o \left(\frac{E \bar{\epsilon}_p}{\beta \sigma_o} \right)^n. \quad (1)$$

where $\bar{\sigma}_{\text{flow}}$ is the effective stress (defined as $\sqrt{\frac{2}{3} s_{ij} s_{ij}}$, where s_{ij} is the stress deviator), σ_o is the uniaxial yield stress, $\bar{\epsilon}_p$ is the effective plastic strain (defined as $\sqrt{\frac{2}{3} \epsilon_{ij} \epsilon_{ij}}$), E is Young's modulus, n is the work-hardening exponent, and β is an empirical prefactor of order unity ($\beta = 3/7$ in the original Ramberg-Osgood formulation [12]).

The asymptotic stress field in the vicinity of the crack tip is taken from solutions presented by Hutchinson [13] and Rice and Rosengren [14], henceforth referred to as HRR. The effective stress about the crack tip is

$$\bar{\sigma} = \sigma_o \left(\frac{\xi}{\beta I_n r \sigma_o^2} \right)^{n/(1+n)} \bar{\sigma}_e(\theta, n), \quad (2)$$

where r is the distance ahead of the crack tip and $K_{I,x}$ is the applied, or far-field, stress intensity factor that characterizes the elastic field well beyond the plastic zone. (We assume small-scale yielding, wherein the plastic zone remains small in relation to other length scales in the problem.) The parameter ξ characterizes the state of constraint, taking on the value 1 for plane stress and $1 - v^2$ for plane strain, where v is Poisson's ratio. The factors $\bar{\sigma}_e$ and I_n are weak functions of the work-hardening exponent, and are determined numerically in the HRR formulation.[†]

2.2. Crack-tip strain-gradient plasticity (HRR-type field)

As for any asymptotic continuum formulation, the HRR field nominally extends to the very crack tip. However, highly nonlinear behavior at the atomic length scale supersedes the attainment of singular stresses. To avoid unphysical stresses in such regions, realistic interatomic potentials have been employed by previous researchers [15]. Presently, we show that under certain conditions the validity of conventionally accepted continuum asymptotic fields can break down at substantially larger-than-atomic length scales.

Recently, Fleck *et al.* [16] have noted that, in the presence of large plastic strain gradients, conventional plasticity formulations must be severely modified at length scales far exceeding atomic dimensions—usually of the order of 1 μm. (More detailed discussion of the theoretical and experimental basis of strain-gradient plasticity is found in Ref. [16] and references therein.) As we shall describe below, the strain-gradient concept defines a length

scale within which the flow strength of the material exceeds the magnitude of the singular stress field. This length scale, which has hitherto been ill-defined in the application of plasticity theory to cracks, allows a self-consistent estimate of the core size.

The local flow strength of a plastically deforming material is related to the local dislocation density, ρ_T , through a modified Orowan-Taylor relation [17–20]

$$\bar{\sigma}_{\text{flow}} = \alpha E b \sqrt{\rho_T}, \quad (3)$$

where α is a constant prefactor of order unity, E is Young's modulus, and b is the magnitude of the Burgers vector. In conventional crystal hardening theory, all of the dislocations are “statistically stored,” whether they existed prior to deformation or arose during deformation via various dislocation-generating sources. However, as argued by Ashby [21], an additional distribution of dislocations is

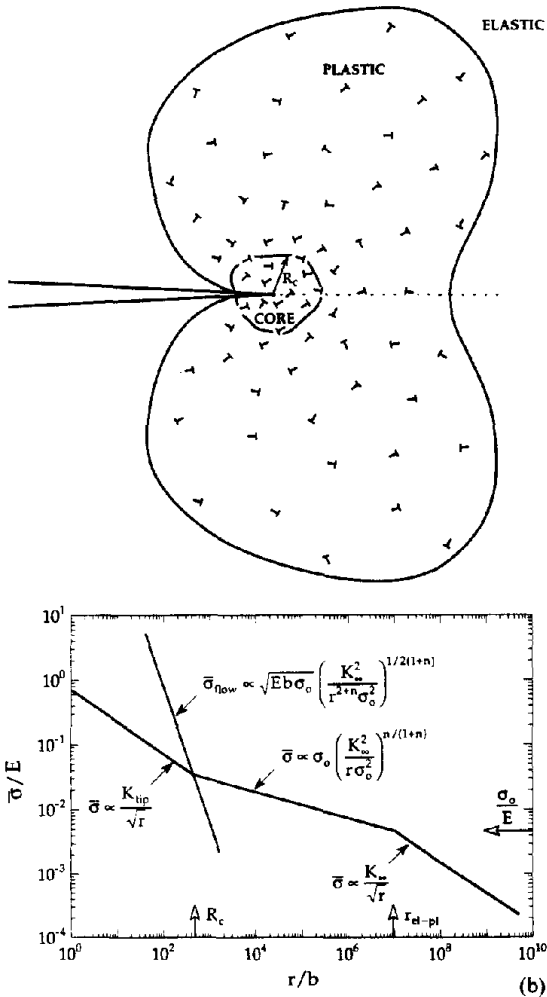


Fig. 1. Schematic illustration of the fracture model. (a) The plastic zone surrounding a remotely loaded, sharp crack. (b) Idealized stress distribution ahead of the crack tip. As the crack tip is approached, one moves from the far-field K -dominant region to the plastically deforming zone and finally to the core region. Enforcement of stress continuity defines the location of the boundary between the core and surrounding plastic zone.

[†]The fourth-order o.d.e. was solved on a Silicon Graphics workstation using a shooting method similar to that described in Refs [13] and [14].

"geometrically necessary" to maintain displacement compatibility in spatially gradient strain fields. Therefore, the total dislocation density is the sum of the statistically stored and geometrically necessary densities ($\rho_T = \rho_G + \rho_S$). In fact, where local strain gradients become large—as will be shown to occur near crack tips—the geometrically necessary dislocation density can far exceed the statistically stored contribution ($\rho_G \gg \rho_S$), allowing the flow strength in such regions to be estimated as

$$\sigma_{\text{flow}} \approx \alpha E b \sqrt{\rho_G}. \quad (4)$$

For isotropic plasticity following J_2 -deformation theory, the density of geometrically necessary dislocations is directly proportional to the effective curvature, χ_e :

$$\rho_G \approx \frac{\chi_e}{b}. \quad (5)$$

The effective curvature represents the scalar magnitude of the plastic component of the curvature tensor, χ_e^{pl} , in a manner similar to the relation between effective strain and the strain tensor†

$$\chi_e = \sqrt{\frac{2}{3} \chi_m^{\text{pl}} \chi_m^{\text{pl}}}. \quad (6)$$

The curvature tensor is, in turn, related to the plastic strain field, ε^{pl}

$$\chi_m^{\text{pl}} = e_{ijk} \varepsilon_{j,k}^{\text{pl}}, \quad (7)$$

where e_{ijk} is the permutation tensor (defined in the Appendix) and

$$\varepsilon_{j,k}^{\text{pl}} \equiv \frac{\partial \varepsilon_j^{\text{pl}}}{\partial x_k}.$$

For a crack exhibiting an HRR singularity, the asymptotic strain field is

$$\varepsilon_{ij}^{\text{pl}} = \frac{\beta \sigma_o}{E} \left(\frac{\xi}{\beta I_n} \frac{K_{1,\infty}^2}{r \sigma_o^2} \right)^{1/(1+n)} \tilde{\varepsilon}_{ij}(\theta, n), \quad (8)$$

from which the effective curvature field for an HRR singularity can be calculated explicitly

$$\chi_e = \sqrt{\frac{2}{3}} \frac{\beta \sigma_o}{E} \left(\frac{\xi}{\beta I_n} \frac{K_{1,\infty}^2}{r^{2+n} \sigma_o^2} \right)^{1/(1+n)} \tilde{\nabla}_e(\theta, n). \quad (9)$$

The function $\tilde{\nabla}_e$ results from differentiation of the angular functions $\tilde{\varepsilon}_{ij}$, as described in the Appendix. Combining equations (4), (5) and (9), we can identify the asymptotic strain-gradient induced hardening distribution about the crack tip

$$\sigma_{\text{flow}} = (\frac{2}{3})^{1/4} \alpha \sqrt{\beta \tilde{\nabla}_e b \sigma_o E} \left(\frac{\xi}{\beta I_n} \frac{K_{1,\infty}^2}{r^{2+n} \sigma_o^2} \right)^{1/2(1+n)}. \quad (10)$$

2.3. The core

From equation (10) we find that the rate of hardening due to geometrically necessary dislocations diverges as the crack tip is approached. For realistic values of the work-hardening exponent (n ranging from 0 to 0.5), the flow strength attains an approximately inverse- r singularity. Meanwhile, the HRR asymptotic solution predicts that the stress field has *at most* an inverse- \sqrt{r} singularity (LEFM), with no singularity whatsoever in the limit of perfect plasticity [exponent is $-n/(1+n)$ for HRR]. Thus, approaching the crack tip, the rate of increase of the flow strength exceeds the divergence of the stress field. As a consequence, a point is reached at which material sufficiently close to the crack tip can no longer plastically deform under the prevailing crack-tip stress field. This condition is analogous to the definition of the elastic core in the previous model; to retain generality, the characteristic dimension thus defined is henceforth referred to simply as "the core".

To this point, the crack tip has been tacitly assumed to be stable against dislocation emission. We defer consideration of the consequences inherent to this assumption until the Discussion section. In the absence of dislocation emission, the stress field inside the core retains an elastic singularity described by a crack-tip stress intensity factor, K_{tip} [8]. (Note that the assumptions just made rely on the additional condition that the elastic core remain large enough compared to atomic dimensions for continuum elasticity theory to be valid.) The effective stress in the immediate vicinity of the crack tip can therefore be evaluated from linear-elastic fracture mechanics (LEFM)

$$\bar{\sigma} = \lambda(\theta) \frac{K_{\text{tip}}}{\sqrt{r}}. \quad (11)$$

The angular dependence of the stress field is conveyed through the function λ , where $2\sqrt{\pi}\lambda/\cos(\theta/2)$ is $\sqrt{8r^2 - 8r + 5 - 3\cos(\theta)}$ for plane strain and $\sqrt{5 - 3\cos(\theta)}$ for plane stress.

2.4. Core size and shielding ratio

It remains to establish the location of the boundary across which the scaling of the stress field switches from HRR [equation (2)] to LEFM [equation (11)], and subsequently to evaluate the degree of crack-tip shielding afforded by the plastic zone.

At the point of incipient fracture, the crack-tip stress intensity must attain its critical value, K_c^{tip} . Using the Irwin relation, we can restate the fracture criterion in terms of the critical energy release rate, G_c^{tip}

$$K_{\text{tip}} \rightarrow \sqrt{\frac{1}{\xi} G_c^{\text{tip}} E}, \quad (12)$$

where G_c^{tip} is the inherent Griffith toughness. The value of G_c^{tip} is simply the work of adhesion, W_{ad} , of

†Henceforth, Einstein summation convention over repeated indices is assumed.

the solid-solid interface—a material parameter that can be calculated from atomistic models or estimated using various experimental techniques.

As seen from Fig. 1(b), the location of the interface corresponds to the crossover point at which the flow strength [equation (10)] exceeds the stress attainable in a homogeneous HRR crack-tip field. (This empirical construction does not in itself guarantee compatibility, but has been used in limited circumstances to provide boundary conditions at elastic-plastic interfaces.) At distances closer to the crack tip than the core length, the stress is insufficient to induce plastic flow and the stress field is described by equation (11). Equations (2), (10) and (11) represent a system of three equations in three unknowns. Enforcing continuity of effective stress across the core boundary, $r = R_c$, along a fixed direction (say $\theta = 0$), we find that

$$\frac{R_c}{b} = \left(\frac{g_n E}{\tilde{\sigma}_c^2 \sigma_o} \right) \left(\frac{\lambda^2}{g_n \xi} \frac{W_{ad}}{b \sigma_o} \right)^{1-2n} \quad (13)$$

and

$$\frac{g_c^x}{W_{ad}} = \left(\frac{\beta I_n}{\tilde{\sigma}_c^2} \frac{\lambda^2}{\xi} \right) \left(\frac{\lambda^2}{g_n \xi} \frac{W_{ad}}{b \sigma_o} \right)^{1-n}, \quad (14)$$

where g_c^x/W_{ad} defines the crack-tip shielding ratio. For conciseness, we define $g_n \equiv \sqrt{\frac{2}{3}} \alpha^2 \beta \tilde{\sigma}_c$, where the subscript n serves to emphasize the functional dependence of g on the work-hardening exponent.

2.5. Thermal effects

Thus far, the thermal contribution to the flow strength has been neglected. Adding a thermal component, $\sigma^*(T)$, to equation (4), we find that the shielding ratio must satisfy

$$\begin{aligned} \frac{\sqrt{g_n \xi}}{\lambda} \left(\frac{W_{ad}}{b \sigma_o} \right)^{-1/2} & \left(\kappa \frac{g_c^x}{W_{ad}} \right)^{1/2(1-n)} \\ + \frac{\sigma^*}{\tilde{\sigma}_c \sigma_o} \left(\kappa \frac{g_c^x}{W_{ad}} \right)^{-n/(1-n)} & = 1, \quad (15) \end{aligned}$$

where

$$\kappa \equiv \frac{\xi}{I_n \beta} \left(\frac{\tilde{\sigma}_c}{\lambda} \right)^2.$$

The temperature dependence of σ^* can be written [18, 22]

$$\sigma^*(T) = \sigma^*(0) \left(1 - \frac{T}{T_c(\dot{\epsilon})} \right), \quad (16)$$

where T is the absolute temperature and T_c defines the critical temperature above which there is sufficient thermal energy to overcome barriers to dislocation

Table I. Selected values of HRR parameters under plane strain and plane stress conditions for $\theta = 0$

n	Plane strain			Plane stress		
	$\tilde{\sigma}_c$	I_n	\tilde{V}_c	$\tilde{\sigma}_c$	I_n	\tilde{V}_c
0.0	1	3.7	—	1	2.5	—
0.1	0.67	4.5	0.039	1.00	3.0	0.90
0.2	0.46	5.0	0.059	0.99	3.4	0.95
0.3	0.30	5.4	0.070	0.98	3.8	0.96
0.4	0.18	5.7	0.077	0.98	4.0	0.97
0.5	0.09	5.9	0.082	0.97	4.2	0.97

motion by thermal activation alone [e.g. at $T \geq T_c$, $\sigma^*(T) = 0$ and the solutions for shielding ratio and core size revert to those given in equations (13) and (14)]. The thermal component of σ_o is assumed to be much smaller than the overall magnitude of σ_o and is thus neglected. As a final complication, an implicit dependence of $\sigma^*(0)$ on W_{ad} is anticipated in equation (16). The explicit form of this dependence has yet to be determined and is not considered in the present analysis. The dependence of T_c on the strain rate, $\dot{\epsilon}$, is described by an Arrhenius relation through the Helmholtz free energy change, ΔF , required to overcome the barrier to dislocation motion [18, 22]

$$T_c = \frac{\Delta F}{k \ln \left(\frac{bv_d d \rho_m}{\dot{\epsilon}} \right)}, \quad (17)$$

where k is Boltzmann's constant, v_d is the Debye frequency, d is the distance moved by the dislocation for every barrier it overcomes, and ρ_m is the density of mobile dislocations.

3. DISCUSSION

Using appropriate values for the proportionality constants in equations (13) and (14) (Table I), the shielding ratios and core sizes are plotted in Figs 2(a) and (b), respectively, for a range of work-hardening exponents. The core size is generally much larger than the Burger's vector, suggesting that the use of continuum approximations is reasonable. The positive slopes of the shielding ratio curves in Fig. 2(a) indicate that the strain-gradient model *does* predict a synergistic coupling between the macroscopic toughness (attributed to plastic deformation) and the inherent material toughness (represented by the ideal cleavage energy, W_{ad}). Such behavior is in qualitative agreement with observations of segregation-induced embrittlement [23–26], whence a slight reduction in the work of adhesion leads to a dramatic decrease in the macroscopic toughness.

Combining equations (15) and (16), we can plot the temperature dependence of the shielding ratio (Fig. 3). A sharp transition from ductile (high shielding ratio) to brittle (low shielding ratio) behavior is evident. The temperature at which the transition occurs corresponds to the brittle-to-ductile

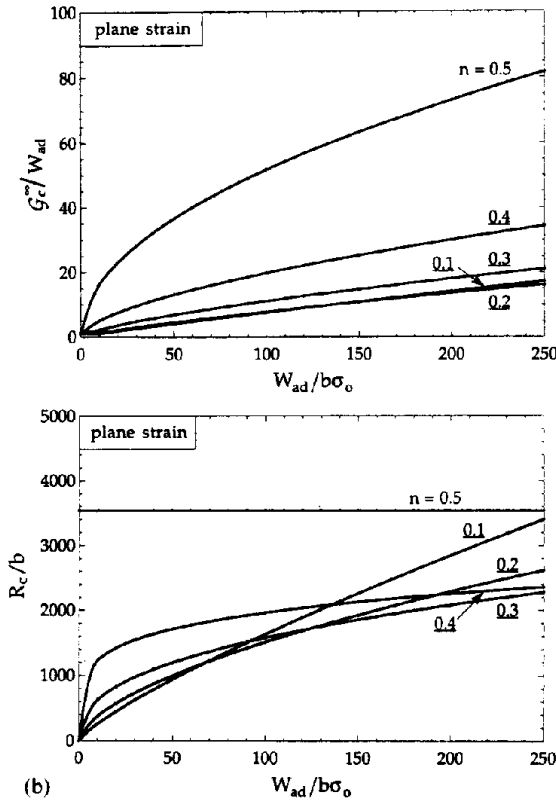


Fig. 2. Variation of (a) shielding ratio and (b) core size with the work of adhesion for a range of work-hardening exponents. All curves were calculated using $\alpha = 1$, $\beta = 3/7$, $\nu = 1/3$ and $E/\sigma_0 = 1000$.

transition temperature, below which background dislocation mobility is effectively frozen out (i.e. the thermal activation, kT , falls sufficiently below the activation energy for overcoming the lattice stress). As expected, the transition occurs more readily for materials having a greater thermal sensitivity of flow strength [larger $\sigma^*(0)$]. As described in the previous section, the lack of an explicit relationship between

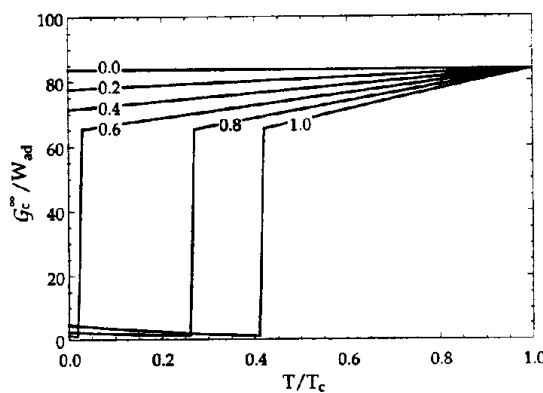


Fig. 3. Dependence of the shielding ratio on temperature for varying values of the ratio $\sigma^*(0)/\sigma_c \sigma_0$, illustrating the onset of a ductile-to-brittle transition associated with suppression of background plasticity.

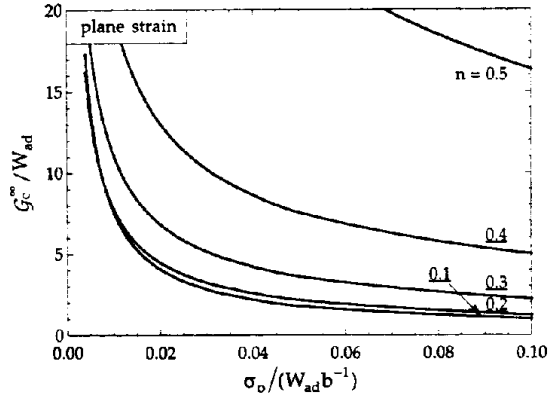


Fig. 4. Strength-toughness dependence predicted on the basis of the strain-gradient model.

$\sigma^*(0)$ and W_{ad} precludes further quantification of the brittle-ductile transition. However, closely associated with the temperature dependence of toughness is strain-rate dependence. As indicated in equation (17), increasing strain rate has the effect of increasing T_c . Setting the absolute temperature constant and steadily increasing the strain rate is therefore analogous to moving from right to left along the curves of Fig. 3. Therefore, materials that are especially susceptible to embrittlement at low temperatures are also expected to behave in a brittle manner at high loading rates.

An interesting implication of the present model is that it predicts the often-observed phenomenon of strength-toughness correlation in plastically deforming materials. This can be illustrated by inverting the abscissa of Fig. 2(a). The resulting plot of toughness as a function of yield strength is shown in Fig. 4. It has long been observed that metal alloys exhibit an inverse relationship between yield strength and fracture toughness [27, 28], but this phenomenon has heretofore eluded quantitative explanation. Specifically, attempts to improve the strength of alloys by work-hardening invariably lead to decreased toughness (conversely, decreasing the yield strength by thermal annealing raises the toughness). Such behavior has been observed in other material systems having a strongly coupled fracture process, such as transformation-toughened zirconia, in which the cohesive energy dictates the extent of the transformation zone [29].

It may be useful at this point to briefly compare the present model to the elastic core formulation of Ref. [11]. Nominally, the two descriptions of the fracture process are very similar. Both models allow for a sharp, Griffith-type crack tip to coexist with background plasticity. Both predict a strong coupling between the crack tip and the surrounding plastic zone, as evidenced by the positive slope of the shielding ratio curves. In both, a characteristic core dimension is determined, within which no plastic deformation occurs. The main distinction between

the two approaches lies in the physical model used to identify the core size.

In the original model, a dislocation-free zone is postulated to exist directly surrounding the crack tip. Using a standard correlation in crystal hardening theory [17], the flow stress is related to the dislocation spacing (or dislocation cell size)

$$\bar{\sigma}_{\text{flow}}^{\max} = \frac{\alpha Eh}{R_c}. \quad (18)$$

$\bar{\sigma}_{\text{flow}}^{\max}$ can be thought of as the maximum effective flow stress to which the material has hardened, expected to occur directly at the interface between the elastic core and the surrounding plastic zone. The shielding ratio based on this relation is [11]

$$\frac{G_c}{W_{\text{ad}}} \propto \left(\frac{W_{\text{ad}}}{b\sigma_o} \right)^{(1-n)/n}, \quad (19)$$

and the core size at initiation of fracture is

$$\frac{R_c}{b} \propto \frac{E}{\sigma_o} \left(\frac{W_{\text{ad}}}{b\sigma_o} \right)^{-1}. \quad (20)$$

Note the absence of an explicit dependence of core size on either yield strength or work-hardening coefficient in equation (20).

Although a dislocation-free zone model allows determination of a core dimension, it is based on the tenuous premise that the dislocation spacing immediately surrounding the crack tip is the characteristic length governing the core size. In such a case, the core size is proportional to the distance from the crack tip to the next-nearest dislocation (e.g. $R \propto \rho^{-1/2}$). Strain-gradient plasticity theory, however, suggests that the dislocation spacing is not the characteristic length scale. In fact, the dislocation spacing becomes vanishingly small (continuum limit) approaching the crack tip, inducing strain-gradient hardening local to the crack tip. In general, then, the core encompasses a large number of immobile dislocations and the length scale is therefore determined not by the dislocation spacing but by the strain gradient.

Although the model presented above allows for a relatively sweeping characterization of a class of fracture problems, several issues remain to be addressed. These are: (1) dislocation emission from the crack tip; (2) breakdown of continuum asymptotic solutions at both very fine and very large length scales; and (3) the discrepancy between dislocation and continuum plasticity formulations. Although we make no attempt to resolve these issues in the present contribution, their consideration may prove critical in subsequent attempts at bringing theoretical and experimental results into closer agreement.

The first point refers to the apparent neglect of possible dislocation emission in the preceding analysis. Identifying the criterion for dislocation

emission from the crack tip with a critical ratio of unstable stacking fault energy to work of adhesion [30], we can superimpose the criterion for first dislocation emission (a vertical line) on Fig. 2(a). However, satisfaction of the criterion for first dislocation emission does not in itself preclude the ability of the fracture process to proceed in a cleavage-type manner. In fact, the criterion for subsequent emission is expected to be more conservative due to the back stress from the emitted dislocation, while a singular stress is still retained at the singly-blunted crack tip, facilitating the propagation of a cleavage crack [31]. Therefore, although moderate dislocation emission is expected to perturb the stress field directly adjacent to the crack tip [$r/b \approx 1$ in Fig. 1(b)], the cleavage process may still proceed in approximate accordance with the present model.

The second limitation refers to the simplifying assumptions made in identifying the stress field ahead of the crack tip. As stated from the start, the present analysis is founded on a small-scale yielding approximation in order to simplify the description of the loading field. Perhaps more restrictive is the use of asymptotic solutions to the stress and strain fields. Clearly, higher-order terms can affect the estimates of the core size and shielding ratio. Similarly, an error is introduced in our neglect of statistically stored dislocations in equation (4), with the consequence of slightly underestimating the flow strength. Lastly, the strain-gradient material is embedded within the plastic zone without any modification of the prevailing stress fields. A fully consistent treatment—though likely to be analytically intractable—may provide improved accuracy in attempts to make direct comparisons with experimental data [32].

The final issue for concern refers to the apparent incongruity between the dislocation plasticity treatment [as epitomized by the Taylor relation, equation (4)] and continuum plasticity [e.g. Ramberg–Osgood constitutive property, equation (1)]. Dislocation plasticity makes no allowances for “weak” or “strong” interactions between dislocations. In fact, the only constitutive behavior fully consistent with the Orowan–Taylor relation is parabolic hardening. On the other hand, continuum plasticity makes allowances for a wide range of hardening behavior, ranging from perfectly-plastic ($n = 0$) to parabolic ($n = 0.5$). To some extent, the resolution to this apparent inconsistency is simply to allow each constitutive description to govern over the length scale for which it was intended. At the dislocation scale, discrete dislocation–dislocation interactions must lead to *local* resistance to flow according to equation (4). At the macroscopic scale, various dislocation accommodation and relaxation mechanisms can reduce the apparent flow resistance from the parabolic limit. Where the deformation-free core is involved (length scales $< 10^4 b$), the use of a dislocation-based model [equation (4)] seems

justified. In describing the surrounding elastic-plastic field (length scales $\gg 10^4 b$), the use of a continuum-based model [equations (1) and (2)] seems equally justified.

4. SUMMARY

We have proposed that a number of fracture phenomena exhibiting cleavage-type fracture in the presence of dislocation plasticity can be explained on the basis of a simple model accounting for the coupling between the plastic deformation and the ideal (Griffith) fracture energy. Specifically, our results show that the effect of ideal fracture energy on the plastic dissipation is synergistic, with slight variations in Griffith energy affecting order-of-magnitude changes in toughness. Further, we suggest a means by which temperature and strain-rate effects can be incorporated, demonstrating the capacity of the model to predict sharp transitions from ductile to brittle fracture regimes. Suggested applications of the model include segregation-induced embrittlement observed in a number of metals and metal-ceramic interfaces, the ductile-to-brittle transition in both metals and ceramics, the strain-rate dependence of fracture toughness and the strength-toughness correlation in metals.

Acknowledgements—The authors would like to thank L. M. Brown (Cambridge) for helpful discussions leading to the preparation of this manuscript. DML thankfully acknowledges the ONR for his NDSEG Fellowship and GEB would like to acknowledge support from the LLNL Seaborg Institute for Transactinium Science. This work was partially supported by the MRL program of the National Science Foundation under award #DMR-9123048.

REFERENCES

1. A. A. Griffith, *Phil. Trans. R. Soc. Lond. A* **221**, 163 (1920).
2. G. Hahn, M. Kanninen and A. Rosenfeld, *A. Rev. Mater. Sci.* **2**, 381 (1970).
3. R. M. McMeeking, *J. Mech. Phys. Solids* **25**, 357 (1977).
4. E. Orowan, *Trans. Inst. Engrs. Shipbuilders Scot.* **89**, 165 (1945).
5. J. R. Rice, *Proc. 1st Int. Conf. Fracture* (edited by T. Yokobori, T. Kawasaki and J. L. Swedlow), p. 309. Sendai, Japan (1966).
6. E. D. Hondros and M. P. Seah, *Int. Metals Rev.* **22**, 262 (1977).
7. A. G. Evans and B. J. Dalgleish, *Mater. Sci. Engng A* **162**, 1 (1993).
8. R. Thomson, *J. Mater. Sci.* **13**, 128 (1978).
9. Z. Suo, C. F. Shih and A. G. Varias, *Acta metall. mater.* **41**, 1551 (1993).
10. M. L. Jokl, V. Vitek and C. J. McMahon Jr., *Acta metall. mater.* **28**, 1479 (1980).
11. D. M. Lipkin and G. E. Beltz, *Acta mater.* **44**, 1287 (1996).
12. W. Ramberg and W. R. Osgood, National Advisory Committee on Aeronautics (NACA), TN 902 (1943).
13. J. W. Hutchinson, *J. Mech. Phys. Solids* **16**, 13 & 337 (1968).
14. J. R. Rice and G. F. Rosengren, *J. Mech. Phys. Solids* **16**, 1 (1968).
15. G. I. Barenblatt, *Adv. appl. Mech.* **7**, 55 (1962).
16. N. A. Fleck, G. M. Müller, M. F. Ashby and J. W. Hutchinson, *Acta metall. mater.* **42**, 475 (1994).
17. G. I. Taylor, *Proc. R. Soc. Lond. A* **145**, 362 (1934).
18. D. Hull and D. J. Bacon, *Introduction to Dislocations*, 3rd ed., p. 243. Pergamon Press, New York (1989).
19. G. E. Beltz, J. R. Rice, C. F. Shih and L. Xia, *Acta metall. mater.* **44**, 3943 (1996).
20. M. Döner, H. Chang and H. Conrad, *J. Mech. Phys. Solids* **22**, 555 (1974).
21. M. F. Ashby, *Phil. Mag.* **21**, 413 (1970).
22. A. Seeger, *Dislocations and Mechanical Properties of Crystals* (edited by J. C. Fisher, W. G. Johnston, R. Thomson and T. Vreeland, Jr.), p. 243. John Wiley and Sons, New York (1957).
23. J. P. Hirth and J. R. Rice, *Metall. Trans. A* **11**, 1501 (1980).
24. J. S. Wang and P. M. Anderson, *Acta metall. mater.* **39**, 779 (1991).
25. D. Korn, G. Elssner, H. F. Fischmeister and M. Rühle, *Acta metall. mater.* **40**, s355 (1992).
26. D. M. Lipkin, D. R. Clarke and A. G. Evans, unpublished work (1994).
27. A. J. Birkle, R. P. Wei and G. E. Pellissier, *Trans. ASM* **59**, 981 (1966).
28. R. W. Hertzberg, *Deformation and Fracture Mechanics of Engineering Materials*, 2nd ed., p. 353. John Wiley & Sons, New York (1983).
29. M. V. Swain and L. R. F. Rose, *J. Am. Ceram. Soc.* **69**, 511 (1986).
30. J. R. Rice, *J. Mech. Phys. Solids* **40**, 239 (1992).
31. L. L. Gann and G. E. Beltz, work in progress.
32. A numerical strain-gradient plasticity treatment of the stress about a crack tip in a plastic solid is currently being carried out by J. W. Hutchinson and co-workers.

APPENDIX

Strain Gradients in a Mode-I HRR Crack-Tip Field
Using the definition of the permutation tensor, e_{nki}

$$e_{nki} \equiv \begin{cases} 0, & n = k, n = j \text{ or } k = j \\ -1, & n, k, j \text{ is an odd permutation of } 1, 2, 3 \\ +1, & n, k, j \text{ is an even permutation of } 1, 2, 3 \end{cases} \quad (\text{A1})$$

it is possible to write out the curvature tensor of equation (7) explicitly in terms of the plastic strain field components†

$$\chi = \begin{bmatrix} \varepsilon_{13,2} - \varepsilon_{12,3} & \varepsilon_{23,2} - \varepsilon_{22,3} & \varepsilon_{31,2} - \varepsilon_{32,3} \\ \varepsilon_{11,3} - \varepsilon_{13,1} & \varepsilon_{21,3} - \varepsilon_{23,1} & \varepsilon_{31,3} - \varepsilon_{33,1} \\ \varepsilon_{12,1} - \varepsilon_{11,2} & \varepsilon_{22,1} - \varepsilon_{21,2} & \varepsilon_{32,1} - \varepsilon_{31,2} \end{bmatrix}. \quad (\text{A2})$$

It should be noted that symmetry of the strain tensor requires that $\varepsilon_{ij} = \varepsilon_{ji}$. Equation (A2) is substantially reduced when the state of constraint is established. For example, because the strain field is uniform along the out-of-plane direction under both plane strain and plane stress conditions, we can set $\varepsilon_{j,j} = 0$ and $\varepsilon_{11} = \varepsilon_{22} = 0$. Furthermore,

†For clarity, the designation "pl" has been omitted. It is implicitly assumed that both the curvature tensor and strain components are associated with plastic deformation.

incompressibility requires that $\varepsilon_{33} = -(\varepsilon_{11} + \varepsilon_{22})$, reducing the curvature tensor under plane stress to

$$\chi = \begin{bmatrix} 0 & 0 & -(\varepsilon_{11,2} + \varepsilon_{22,2}) \\ 0 & 0 & \varepsilon_{11,1} + \varepsilon_{22,1} \\ \varepsilon_{12,1} - \varepsilon_{11,2} & \varepsilon_{22,1} - \varepsilon_{21,2} & 0 \end{bmatrix}, \text{ plane stress.} \quad (\text{A3})$$

Further simplification of the curvature tensor obtains under plane strain conditions, whence $\varepsilon_{13} = \varepsilon_{23} = \varepsilon_{33} = 0$

$$\chi = \begin{bmatrix} 0 & 0 & 0 \\ 0 & 0 & 0 \\ \varepsilon_{12,1} - \varepsilon_{11,2} & \varepsilon_{22,1} - \varepsilon_{21,2} & 0 \end{bmatrix}, \text{ plane strain.} \quad (\text{A4})$$

The respective strain-component derivatives can now be determined using the HRR strain field. Defining an orthogonal basis in cylindrical coordinates such that (x_1, x_2, x_3) corresponds to (r, θ, z) and $(\partial x_1, \partial x_2, \partial x_3)$ to

$$\tilde{\nabla}_c^2 = \begin{cases} \left(\frac{1}{1+n} \tilde{\varepsilon}_{rr} + \tilde{\varepsilon}_{\theta\theta,0} \right)^2 + \left(\frac{1}{1+n} \tilde{\varepsilon}_{\theta\theta} + \tilde{\varepsilon}_{\theta\theta,0} \right)^2 + (\tilde{\varepsilon}_{rr,0} + \tilde{\varepsilon}_{\theta\theta,0})^2 + \left(\frac{1}{1+n} \tilde{\varepsilon}_{rr} + \frac{1}{1+n} \tilde{\varepsilon}_{\theta\theta} \right)^2, & \text{plane stress} \\ \left(\frac{1}{1+n} \tilde{\varepsilon}_{rr} + \tilde{\varepsilon}_{\theta\theta,0} \right)^2 + \left(\frac{1}{1+n} \tilde{\varepsilon}_{\theta\theta} + \tilde{\varepsilon}_{\theta\theta,0} \right)^2, & \text{plane strain} \end{cases}. \quad (\text{A7})$$

$(\hat{r}\hat{r}, r\hat{\theta}\hat{\theta}, \hat{z}\hat{z})$, and combining with the HRR strain field given in equation (8), the relevant derivatives of the strain components can be determined

$$\begin{cases} \varepsilon_{0,1} \\ \varepsilon_{0,2} \end{cases} \equiv \begin{cases} \varepsilon_{rr,r} \\ \frac{1}{r} \varepsilon_{\theta\theta,\theta} \end{cases} = \frac{\beta\sigma_o}{E} \left(\frac{\xi}{\beta I_n} \frac{K_{1,x}^2}{r^{2+n}\sigma_o^2} \right)^{1/(1+n)} \times \begin{cases} \left(\frac{-1}{1+n} \right) \tilde{\varepsilon}_{ij}(\theta, n) \\ \varepsilon_{ij,i}(\theta, n) \end{cases}. \quad (\text{A5})$$

The effective curvature can now be calculated using equations (6) and (A3)–(A5)

$$\chi_e = \sqrt{\frac{2}{3}} \frac{\beta\sigma_o}{E} \left(\frac{\xi}{\beta I_n} \frac{K_{1,x}^2}{r^{2+n}\sigma_o^2} \right)^{1/(1+n)} \tilde{\nabla}_c(\theta, n), \quad (\text{A6})$$

where